

## Tsunami asymptotics

M V Berry<sup>1</sup>

H H Wills Physics Laboratory, Tyndall Avenue, Bristol BS8 1TL, UK

*New Journal of Physics* **7** (2005) 129

Received 4 April 2005

Published 23 May 2005

Online at <http://www.njp.org/>

doi:10.1088/1367-2630/7/1/129

‘There was an awful rainbow once in heaven’ (John Keats, 1820)

**Abstract.** By applying the technique of uniform asymptotic approximation to the oscillatory integrals representing tsunami wave profiles, the form of the travelling wave far from the source is calculated for arbitrary initial disturbances. The approximations reproduce the entire profiles very accurately, from the front to the tail, and their numerical computation is much faster than that of the oscillatory integrals. For one-dimensional propagation, the uniform asymptotics involve Airy functions and their derivatives; for two-dimensional propagation, the uniform asymptotics involve products of these functions. Separate analyses are required when the initial disturbance is specified as surface elevation or surface velocity as functions of position, and when these functions are even or odd.

<sup>1</sup> [http://www.physics.bristol.ac.uk/staff/berry\\_mv.html](http://www.physics.bristol.ac.uk/staff/berry_mv.html)

**Contents**

<b>1. Introduction</b>	<b>2</b>
<b>2. Tsunami wave integrals</b>	<b>3</b>
2.1. One-dimensional propagation . . . . .	3
2.2. Two-dimensional propagation . . . . .	5
<b>3. Uniform approximation map</b>	<b>7</b>
<b>4. Uniform approximations for one-dimensional waves</b>	<b>8</b>
4.1. Even initial elevation . . . . .	8
4.2. Odd initial elevation . . . . .	10
4.3. Even initial velocity . . . . .	11
4.4. Odd initial velocity . . . . .	12
<b>5. Uniform approximations for two-dimensional waves</b>	<b>12</b>
5.1. Even initial elevation . . . . .	12
5.2. Odd initial elevation . . . . .	14
5.3. Even initial velocity . . . . .	15
5.4. Odd initial velocity . . . . .	16
<b>6. Concluding remarks</b>	<b>17</b>
<b>Acknowledgments</b>	<b>18</b>
<b>References</b>	<b>18</b>

**1. Introduction**

Tsunamis are surface water waves that can travel for thousands of kilometres from the disturbance that creates them [1, 2]. Their destructiveness stems from the fact that their energy is concentrated near a front that travels with the maximum group velocity  $\sqrt{gh}$ , where  $h$  (assumed constant) is the depth of the ocean. The profiles of tsunami waves are given by oscillatory integrals [3] (section 2) representing the propagation of the different wavenumbers in the initial disturbance at the surface (which is related in a simple way to the initial disturbance at the bottom [1, 3]).

My purpose here is to obtain accurate analytic expressions for the travelling tsunami profiles generated by arbitrary sources, thereby eliminating the need for numerical evaluation of the oscillatory integrals for each case. The expressions are obtained by an asymptotic theory that gets more accurate the farther the disturbance travels. This is precisely the situation where numerical evaluation is difficult, because the oscillations in the integrals get faster. Numerical evaluation of the analytic approximations is much faster than direct computation of the oscillatory integrals: up to 20 times faster in some of my calculations.

The technique employed is the uniform asymptotic approximation of integrals [4]–[6], based on mapping of the integrand onto a standard form (section 3). This results in an enormous increase of the range of applicability of the formulas, as compared with the ‘transitional approximations’ [2, 7] obtained by naive expansion of the integrands about the travelling front.

There are several simple cases: propagation can be one-dimensional (perpendicular to a linear initial disturbance) (section 4) or two-dimensional (e.g. if the initial disturbance is an explosion) (section 5); the initial disturbance can be specified by the surface elevation or by the velocity; and the initial disturbance can be even or odd under parity.

In the one-dimensional cases (section 4), the tsunami integrals reduce to an Airy function or its derivative, and the uniformization consists of stretching the well-known transitional approximation [7] to fit the wave far behind the front as well as close to it. In the two-dimensional cases (section 5), the uniform approximations involve less familiar products of Airy functions.

The theory is linear and so describes the travelling wave while its elevation is  $z \ll h$ . Therefore, it does not deal with the nonlinear amplification [8] of the tsunami at the seashore, where it is most destructive.

Tsunamis are long waves on shallow water [9], governed by the dispersion relation giving the frequency  $\omega$  as a function of wavenumber  $k$ :

$$\omega(k) = \sqrt{gk \tanh hk} = \sqrt{gh} \left( k - \frac{1}{6} h^2 k^3 + \dots \right). \quad (1.1)$$

The initial disturbance is a superposition of plane waves with different wavevectors  $\mathbf{k}$  (length  $|\mathbf{k}| = k$ ), whose energy propagates with the group velocity

$$\mathbf{v}_g(k) = \nabla_{\mathbf{k}} \omega(k) = \mathbf{e}_{\mathbf{k}} \sqrt{gh} \left( 1 - \frac{1}{3} (hk)^2 + \dots \right), \quad v_g(0) = \sqrt{gh} \equiv v_{g0}, \quad (1.2)$$

where  $\mathbf{e}_{\mathbf{k}}$  is the direction of  $\mathbf{k}$  and  $v_{g0}$  is the maximum group speed, i.e. the speed with which the front travels. The tsunami profile results from the interference of these plane waves.

The maximum group velocity leads to the concentration of tsunami energy near the front, which is a caustic in spacetime, on which the density of contributing  $k$  values rises to infinity. Rainbows are caustics too (in the space of directions in the sky [10, 11]), leading to the expectation that tsunami profiles will involve the familiar Airy functions that describe the diffraction details in rainbows. And so they do, but in the two-dimensional case the Airy functions appear in a less familiar way, as products. In light of the disastrous tsunami of 26 December 2004 (which stimulated the present study), the analogy with rainbows gives a sinister resonance to the quotation from Keats at the beginning of this paper.

## 2. Tsunami wave integrals

### 2.1. One-dimensional propagation

For one-dimensional propagation, the surface wave elevation  $z(x, t)$  is [3]

$$\begin{aligned} z(x, t) &= \operatorname{Re} \frac{1}{2\pi} \int_{-\infty}^{\infty} dk \left( \bar{z}(k) + i \frac{\bar{\dot{z}}(k)}{\omega(|k|)} \right) \exp\{i(kx - \omega(|k|)t)\} \\ &\equiv z_1(x, t) + z_2(x, t), \end{aligned} \quad (2.1)$$

where the subscripts 1 and 2 refer to contributions from the initial elevation  $z(x, 0)$  and the initial velocity  $\dot{z}(x, 0)$ , expressed in terms of their Fourier transforms:

$$\bar{z}(k) = \int_{-\infty}^{\infty} dx z(x, 0) \exp\{-ikx\}, \quad \bar{\dot{z}}(k) = \int_{-\infty}^{\infty} dx \dot{z}(x, 0) \exp\{-ikx\}. \quad (2.2)$$

Reality of the elevation implies that the real part of the Fourier transforms is even and the imaginary part is odd, that is

$$\operatorname{Re} \bar{z}(k) = \operatorname{Re} \bar{z}(-k), \quad \operatorname{Im} \bar{z}(k) = -\operatorname{Im} \bar{z}(-k), \quad (2.3)$$

and similarly for the velocity. (Together with (2.1), these relations guarantee that  $z(x, 0) = 0$  if  $\bar{z}(k) = 0$ , and  $\dot{z}(x, 0) = 0$  if  $\dot{\bar{z}}(k) = 0$ .)

It will simplify subsequent calculations to work in terms of dimensionless variables

$$\Delta \equiv v_{g0}t/h, \quad \xi \equiv x/(v_{g0}t), \quad \kappa \equiv hk. \quad (2.4)$$

Here  $\Delta$  is the scaled time, represented by distance from the source to the travelling front, in units of  $h$ ;  $\xi$  is the scaled distance, represented by distance from the source in units of distance to the front (thus  $\xi = 1$  is the position of the front);  $\kappa$  is the corresponding scaled wavenumber. With corresponding scalings for the elevation and velocity, namely

$$\begin{aligned} \zeta(\xi, \Delta) &\equiv \frac{z(x, t)}{h}, & \dot{\zeta}(\xi, \Delta) &\equiv \frac{\dot{z}(x, t)}{v_{g0}}, \\ \bar{\zeta}(\kappa) &\equiv \frac{1}{h^2} \bar{z}(k), & \dot{\bar{\zeta}}(\kappa) &\equiv \frac{1}{hv_{g0}} \dot{\bar{z}}(k), \end{aligned} \quad (2.5)$$

the two contributions to (2.1) become

$$\begin{aligned} \zeta_1(\xi, \Delta) &= \operatorname{Re} \frac{1}{2\pi} \int_{-\infty}^{\infty} d\kappa \bar{\zeta}(\kappa) \exp\{i\Delta(\kappa\xi - \sqrt{|\kappa \tanh \kappa|})\} \\ \zeta_2(\xi, \Delta) &= \operatorname{Re} \frac{1}{2\pi} \int_{-\infty}^{\infty} d\kappa \frac{i\dot{\bar{\zeta}}(\kappa)}{\sqrt{|\kappa \tanh \kappa|}} \exp\{i\Delta(\kappa\xi - \sqrt{|\kappa \tanh \kappa|})\}. \end{aligned} \quad (2.6)$$

We will obtain asymptotic approximations for  $\Delta \gg 1$ , giving the form of the tsunami long after the initial disturbance.

It is convenient to separate the even and odd parts E and O from the two contributions using (2.3), giving

$$\zeta_{1E}(\xi, \Delta) = \frac{1}{\pi} \int_0^{\infty} d\kappa \bar{\zeta}_E(\kappa) \cos(\Delta\kappa\xi) \cos(\Delta\sqrt{\kappa \tanh \kappa}), \quad (2.7)$$

$$\zeta_{1O}(\xi, \Delta) = -\frac{1}{\pi} \int_0^{\infty} d\kappa \operatorname{Im} \bar{\zeta}_O(\kappa) \sin(\Delta\kappa\xi) \cos(\Delta\sqrt{\kappa \tanh \kappa}), \quad (2.8)$$

$$\zeta_{2E}(\xi, \Delta) = \frac{1}{\pi} \int_0^{\infty} d\kappa \frac{\dot{\bar{\zeta}}_E(\kappa)}{\sqrt{|\kappa \tanh \kappa|}} \cos(\Delta\kappa\xi) \sin(\Delta\sqrt{|\kappa \tanh \kappa|}), \quad (2.9)$$

$$\zeta_{2O}(\xi, \Delta) = -\frac{1}{\pi} \int_0^{\infty} d\kappa \frac{\operatorname{Im} \dot{\bar{\zeta}}_O(\kappa)}{\sqrt{\kappa \tanh \kappa}} \sin(\Delta\kappa\xi) \sin(\Delta\sqrt{\kappa \tanh \kappa}). \quad (2.10)$$

Realistic disturbances may not possess symmetry, and would need to be modelled by a superposition of these contributions.

The four integrals, and also their two-dimensional counterparts to be studied in section 2.2, are all related: for example,  $\zeta_{10}$  is the derivative of  $\zeta_{1E}$  with respect to  $\xi$  for a suitable choice of  $\bar{\zeta}_{1E}(\kappa)$ . Nevertheless, it will be convenient to treat them separately.

For the initial conditions, we can choose  $\bar{\zeta}_E(\kappa)$  to be any even function of  $\kappa$ , and  $\bar{\zeta}_O(\kappa)$  and  $\bar{\zeta}'_O(\kappa)$  to be any odd functions of  $\kappa$ . But the ‘velocity-even’ function  $\bar{\zeta}_E(\kappa)$  must vanish at  $\kappa = 0$ ; this is to ensure that the integrated initial velocity is zero—a necessary condition for incompressible water, for which finite integrated initial velocity would imply an inward flow at infinity. Indeed, if (2.9) is computed for a choice of  $\bar{\zeta}_E(\kappa)$  that does not vanish at  $\kappa = 0$ , the tsunami profile has an unphysical finite-elevation tail extending back from the front to the source. This has some mathematically interesting features, but we do not discuss them here.

In numerical comparisons of these exact expressions with the asymptotic approximations to be obtained in subsequent sections, we choose even and odd initial surface disturbances in the forms of Gaussians

$$\bar{\zeta}_E(\kappa) = \exp(-\frac{1}{2}\kappa^2 w^2), \quad \bar{\zeta}_O(\kappa) = \bar{\zeta}'_O(\kappa) = i\kappa \exp(-\frac{1}{2}\kappa^2 w^2), \quad \bar{\zeta}_E(\kappa) = \kappa^2 \exp(-\frac{1}{2}\kappa^2 w^2). \quad (2.11)$$

The parameter  $w$  represents the lateral extent of the initial disturbance, measured in units of  $h$ . These Gaussians are not intended to represent realistic initial disturbances. However, it should be pointed out that bottom disturbances with wavenumber  $k$  are attenuated at the surface by a factor proportional to  $1/\cosh(kh)$  [1], so that bottom disturbances (even discontinuous ones) become analytic at the surface. I have checked the accuracy of the uniform approximations for a variety of different initial conditions in addition to (2.11).

Figure 1 shows some sample numerical computations of the tsunami integrals (2.7)–(2.10). For a depth of 4 km, these correspond to an initial disturbance of 4 km wide and a time of about 1000 s after the initial disturbance, when the front has moved 200 km from the source. It is clear that a variety of tsunami shapes, in which for example the largest wave is not the one that arrives first or where a trough arrives first, can be modelled by superposing contributions of this sort.

For reasons that will be clear later, the profile  $\zeta_{1E}(\xi, \Delta)$  looks similar to  $-\zeta_{10}(\xi, \Delta)$ , and the profile  $\zeta_{10}(\xi, \Delta)$  looks similar to  $\zeta_{1E}(\xi, \Delta)$ , but they are not identical. A similar remark applies to the two-dimensional case.

## 2.2. Two-dimensional propagation

For a source localized in two dimensions, the superpositions for the wave  $z(\mathbf{r}, t)$ , where  $\mathbf{r} = (x, y)$ , involve two-dimensional wavevectors  $\mathbf{k}$ . We use scalings analogous to (2.4), with scaled position

$$\boldsymbol{\rho} \equiv \mathbf{r}/(v_{g0}t), \quad \boldsymbol{\rho} = \{\rho, \phi\}. \quad (2.12)$$

Thus the front corresponds to the circle  $\rho = 1$ . The wave integrals analogous to (2.6) are

$$\begin{aligned} \zeta_1(\boldsymbol{\rho}, \Delta) &= \text{Re} \frac{1}{(2\pi)^2} \iint_{\kappa \text{ plane}} d\boldsymbol{\kappa} \bar{\zeta}(\boldsymbol{\kappa}) \exp\{i\Delta(\boldsymbol{\kappa} \cdot \boldsymbol{\rho} - \sqrt{|\boldsymbol{\kappa} \tanh \boldsymbol{\kappa}|})\}, \\ \zeta_2(\boldsymbol{\rho}, \Delta) &= \text{Re} \frac{1}{(2\pi)^2} \iint_{\kappa \text{ plane}} d\boldsymbol{\kappa} \frac{i\bar{\zeta}'(\boldsymbol{\kappa})}{\sqrt{|\boldsymbol{\kappa} \tanh \boldsymbol{\kappa}|}} \exp\{i\Delta(\boldsymbol{\kappa} \cdot \boldsymbol{\rho} - \sqrt{|\boldsymbol{\kappa} \tanh \boldsymbol{\kappa}|})\}. \end{aligned} \quad (2.13)$$

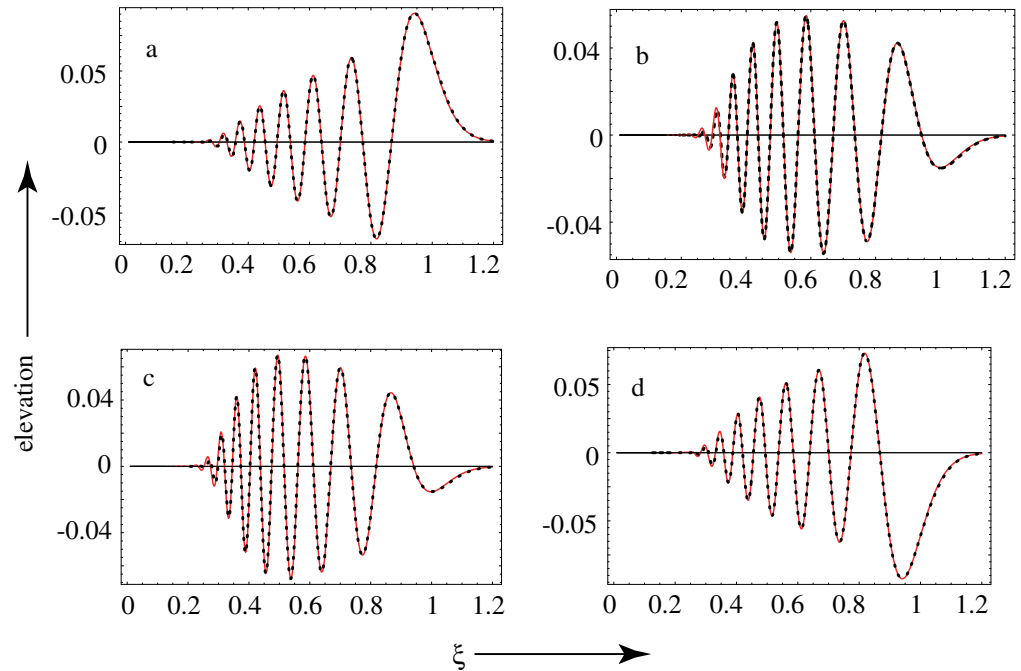


**Figure 1.** One-dimensional tsunami profiles for  $\Delta = 50$ ,  $w = 1$ , calculated for the Gaussian initial conditions (2.11), for (a) even initial elevation  $\zeta_{1E}$ ; (b) odd initial elevation  $\zeta_{1O}$ ; (c) even initial velocity  $\zeta_{2E}$ ; (d) odd initial velocity  $\zeta_{2O}$ . Full red curves, numerical computations of oscillatory integrals (2.7)–(2.10) and dots, uniform asymptotic approximations of section 4, almost indistinguishable from the exact profiles.

As before, it is possible to separate the even and odd contributions. In the analytic theory of section 5, these will be treated in full generality. However, it is convenient now to write explicit formulas for the simplest cases: circularly symmetric parity-even initial disturbances and parity-odd initial disturbances with the angular dependence  $\cos \phi_\rho$ . Thus

$$\begin{aligned} \operatorname{Re} \bar{\zeta}(\kappa) &\equiv f_{1E}(\kappa), & \operatorname{Im} \zeta(\kappa) &= \cos \phi_\kappa f_{1O}(\kappa), \\ \operatorname{Re} \dot{\bar{\zeta}}(\kappa) &\equiv f_{2E}(\kappa), & \operatorname{Im} \dot{\zeta}(\kappa) &= \cos \phi_\kappa f_{2O}(\kappa), \end{aligned} \quad (2.14)$$

where the real function  $f_{1E}(\kappa)$  is finite at  $\kappa = 0$ , the real functions  $f_{1O}(\kappa)$  and  $f_{2O}(\kappa)$  vanish linearly at  $\kappa = 0$ , and, to respect incompressibility (cf the discussion before (2.11)), the real function  $f_{2E}(\kappa)$  vanishes quadratically at  $\kappa = 0$ . The four cases, analogous to (2.7)–(2.10), reduce to the following radial integrals:

$$\zeta_{1E}(\rho, \Delta) = \frac{1}{2\pi} \int_0^\infty d\kappa \kappa f_{1E}(\kappa) J_0(\Delta\kappa\xi) \cos(\Delta\sqrt{\kappa \tanh \kappa}), \quad (2.15)$$

$$\zeta_{1O}(\rho, \Delta) = -\frac{\cos \phi_\rho}{2\pi} \int_0^\infty d\kappa \kappa f_{1O}(\kappa) J_1(\Delta\kappa\xi) \cos(\Delta\sqrt{\kappa \tanh \kappa}), \quad (2.16)$$

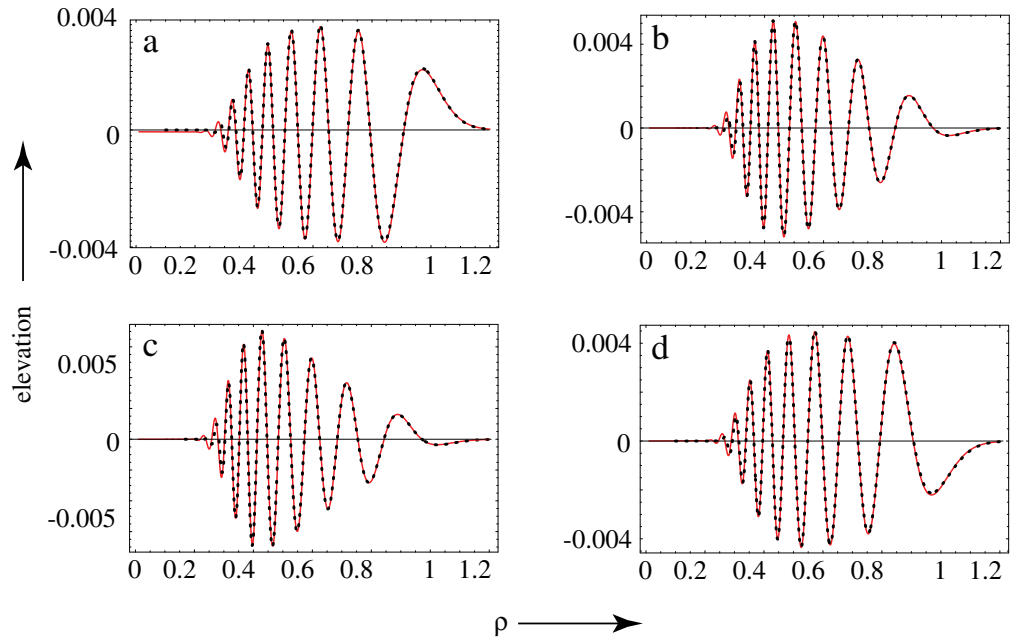


**Figure 2.** Two-dimensional tsunami profiles for  $\Delta = 50$ ,  $w = 1$ , calculated for the Gaussian initial conditions (2.19), for (a) even initial elevation  $\zeta_{1E}$ ; (b) odd initial elevation  $\zeta_{1O}$ ; (c) even initial velocity  $\zeta_{2E}$ ; (d) odd initial velocity  $\zeta_{2O}$ . Full red curves, numerical computations of oscillatory integrals (2.15)–(2.18); and dots, uniform asymptotic approximations of section 5, almost indistinguishable from the exact profiles.

$$\zeta_{2E}(\rho, \Delta) = \frac{1}{2\pi} \int_0^\infty d\kappa \sqrt{\frac{\kappa}{\tanh \kappa}} f_{2E}(\kappa) J_0(\Delta\kappa\xi) \sin(\Delta\sqrt{\kappa \tanh \kappa}), \quad (2.17)$$

$$\zeta_{2O}(\rho, \Delta) = -\frac{\cos \phi_\rho}{2\pi} \int_0^\infty d\kappa \sqrt{\frac{\kappa}{\tanh \kappa}} f_{2O}(\kappa) J_1(\Delta\kappa\xi) \sin(\Delta\sqrt{\kappa \tanh \kappa}). \quad (2.18)$$

For numerical comparisons, we will use (cf (2.11))

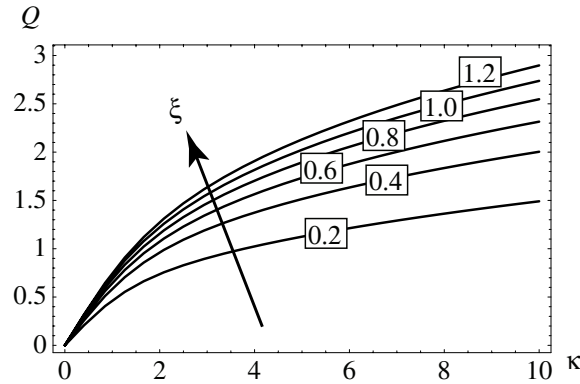
$$\begin{aligned} f_{1E}(\kappa) &= \exp(-\tfrac{1}{2}\kappa^2 w^2), & f_{1O}(\kappa) &= f_{2O} = \kappa \exp(-\tfrac{1}{2}\kappa^2 w^2), \\ f_{2E}(\kappa) &= \kappa^2 \exp(-\tfrac{1}{2}\kappa^2 w^2). \end{aligned} \quad (2.19)$$

Figure 2 shows some numerical illustrations of these tsunami profiles, for the same parameters as in figure 1. This indicates that the one- and two-dimensional wave profiles can be very different, even for similar initial disturbances.

### 3. Uniform approximation map

When  $\Delta \gg 1$  the integrands in (2.6) and (2.13) oscillate rapidly, and we expect the wave to be dominated by the stationary phase points  $\pm\kappa_c(\xi)$ , defined implicitly by

$$\xi = \left( \frac{d}{d\kappa} \sqrt{\kappa \tanh \kappa} \right)_{\kappa=\kappa_c(\xi)}, \quad (3.1)$$



**Figure 3.** Map (3.2) of the integration variable, for the indicated values of  $\xi$ .

corresponding to  $x = v(k_c(x))t$ . In all the subsequent manipulations, the only implicit step is the calculation of  $\kappa_c(\xi)$ . As  $\xi$  increases through unity, the two stationary points approach  $\kappa = 0$ , coalesce and then become imaginary (corresponding to the evanescent disturbance ahead of the tsunami front). We avoid the familiar method of stationary phase [4, 5, 12], because this fails close to the front; we also avoid expanding the integrand about  $\kappa = 0$ , which is valid only very close to the front.

Instead, we map the exponent exactly onto a simpler expression with the same topology of coalescence. The mapping, which will be used in both the one- and two-dimensional cases, consists in changing the integration variable from  $\kappa$  to  $Q$

$$\kappa\xi - \sqrt{\kappa \tanh \kappa} \equiv Q\sigma(\xi) + \frac{1}{3}Q^3. \quad (3.2)$$

To guarantee that the mapping is smooth [6],  $\sigma$  is chosen to make the stationary points coincide, that is

$$\kappa = \kappa_c(\xi) \Leftrightarrow Q = Q_c(\xi) = \sqrt{-\sigma(\xi)}. \quad (3.3)$$

This gives

$$\sigma(\xi) = -\left[\frac{3}{2}(\sqrt{\kappa_c(\xi) \tanh \kappa_c(\xi)} - \kappa_c \xi)\right]^{2/3}. \quad (3.4)$$

Figure 3 shows the mapping from  $\kappa$  for  $Q$  for several values of  $\xi$ , showing that it is smooth, even as  $\xi$  passes through unity. For later reference, we note the form of  $\sigma(\xi)$  near  $\xi = 1$  as

$$\sigma(\xi) = 2^{1/3}(\xi - 1) + \dots. \quad (3.5)$$

## 4. Uniform approximations for one-dimensional waves

### 4.1. Even initial elevation

The product of cosines in the exact integral (2.7) can be written as the sum of two cosines with arguments involving  $\kappa\xi \pm \sqrt{\kappa \tanh \kappa}$ . We neglect the contribution with the + sign because

it oscillates rapidly over the entire integration range. In the other contribution, the change of variables (3.2) gives

$$\zeta_{1E}(\xi, \Delta) \approx \operatorname{Re} \frac{1}{2\pi} \int_0^\infty dQ G_{1E}(Q) \exp\{i\Delta(Q\sigma(\xi) + \frac{1}{3}Q^3)\}, \quad (4.1)$$

where

$$G_{1E}(Q) = \frac{d\kappa}{dQ} \bar{\zeta}_E(\kappa(Q)). \quad (4.2)$$

Because the mapping from  $\kappa$  to  $Q$  is smooth, this function is finite over the integration range.

In this and subsequent cases, the uniform approximation is obtained by replacing  $Q$  in  $G_{1E}$  by its stationary-point value  $Q_c(\xi)$ . The resulting integral is an Airy function, so the uniform approximation is

$$\zeta_{1E\text{uniform}}(\xi, \Delta) = \frac{1}{2\Delta^{1/3}} G_{1E}(Q(\xi)) \operatorname{Ai}\{\Delta^{2/3}\sigma(\xi)\}. \quad (4.3)$$

To calculate the derivative in (4.2), we differentiate the mapping (3.2) twice, to get, at the stationary point,

$$-\left[\frac{d^2}{d\kappa^2} \sqrt{\kappa \tanh \kappa}\right] \left(\frac{d\kappa}{dQ}\right)^2 = 2Q_c(\xi) = 2\sqrt{-\sigma(\xi)}, \quad (4.4)$$

whence

$$\left(\frac{d\kappa}{dQ}\right)_c = 12^{1/6} \frac{[\sqrt{\kappa_c(\xi) \tanh \kappa_c(\xi)} - \kappa_c(\xi)\xi]^{1/6}}{\sqrt{-\frac{d^2}{d\kappa^2} \sqrt{\kappa_c(\xi) \tanh \kappa_c(\xi)}}}. \quad (4.5)$$

The more familiar transitional approximation [7] is obtained by the expansion of all quantities in (4.3) about  $\xi = 1$ . To lowest order, this gives

$$\zeta_{1E\text{transitional}}(\xi, \Delta) = \frac{\bar{\zeta}_E(\sqrt{2(1-\xi)})}{(4\Delta)^{1/3}} \operatorname{Ai}\{2^{1/3}\Delta^{2/3}(\xi-1)\}. \quad (4.6)$$

The usefulness of this formula is not to represent the profile accurately but to indicate the scale of tsunami waves near the front. From the spacing 3.801 of the first two Airy maxima, the distance between the first two tsunami crests scales as

$$\Delta\xi = \frac{3.801}{2^{1/3}\Delta^{2/3}}, \quad \text{i.e. } \Delta x = 3.02(gt^2h^5)^{1/6}. \quad (4.7)$$

Computation of the uniform approximation in the evanescent region  $\xi > 1$  would require evaluation of the mapping (3.1) where the contributing wavenumber  $\kappa(\xi)$  is imaginary (though (4.3) remains real); in practice, however, the transitional approximation is sufficiently accurate in this region, and has been used in the numerical results given below. (This procedure fails for  $\xi \gg 1$ , but the wave is then so weak that inaccuracies are unimportant.)

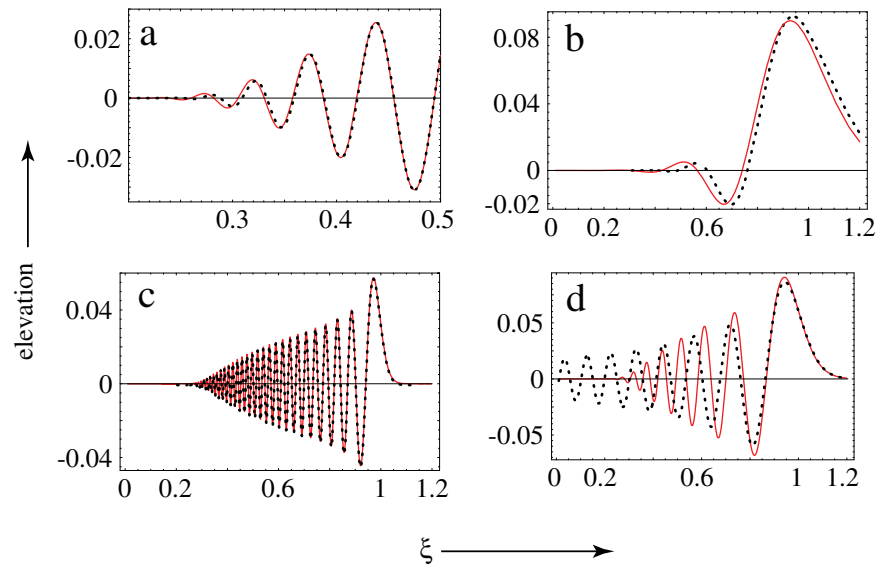


**Figure 4.** One-dimensional tsunami profiles for Gaussian even initial elevations. (a) Magnification of figure 1(a); (b) exact profile (2.7) (full red curve) and uniform approximation (4.3) (dots) for  $w = 2$  and  $\Delta = 20$ ; (c) exact and uniform asymptotic profiles (indistinguishable) for  $w = 1$  and  $\Delta = 200$ ; (d) comparison of exact (full red curve) and transitional (simple Airy) approximation (4.6) (dots), for  $w = 1$  and  $\Delta = 50$ .

In figure 1(a) the error in the uniform approximation is too small to be visible. The magnification in figure 4(a) shows slight discrepancies far behind the front, but overall the agreement is excellent. Figure 4(b) shows a more challenging test of the asymptotics, corresponding to a depth of  $h = 4$  km to an initial profile of 8 km wide, at a time when the front has travelled 80 km from the source. Discrepancies are visible over the whole range, but the overall profile is still well reproduced. For a much larger value of  $\Delta$  in figure 4(c), when the same initial disturbance has reached 800 km, the asymptotic and exact profiles are indistinguishable. Using an unoptimized code and the Airy function routine built into Mathematica<sup>TM</sup>, computation of the uniform asymptotic formula was 20 times faster than the oscillatory integral for the parameters in figure 4(c). By comparison, the transitional Airy approximation fares much less well; as figure 4(d) illustrates, even the first few oscillations are inaccurately reproduced, and the approximation degrades rapidly with increasing distance behind the front.

The accuracy of the uniform approximations for the other one-dimensional cases (sections 4.2–4.4), already illustrated in figures 1(b)–(d), is similar to that just described, so further numerical comparisons will not be presented.

#### 4.2. Odd initial elevation

A similar manipulation of (2.8) leads to

$$\zeta_{1\text{Uniform}}(\xi, \Delta) = \text{Re} \frac{i}{2\pi} \int_0^\infty dQ Q G_{10}(Q) \exp\{i\Delta(Q\sigma(\xi) + \frac{1}{3}Q^3)\}, \quad (4.8)$$

where now

$$G_{10}(Q) = \frac{d\kappa}{dQ} \frac{\text{Im} \bar{\zeta}_0(\kappa(Q))}{Q}. \quad (4.9)$$

This form for  $G_{10}$  is chosen to incorporate the linear vanishing of  $\bar{\zeta}_{10}(\kappa)$  at  $\kappa = 0$ ; thus  $G_{10}$ , like  $G_{1E}$ , is finite over the whole integration range. When  $Q$  is replaced by  $Q_c$ , the integral is the derivative of the Airy function (because of the factor  $Q$  in the integrand), giving the uniform approximation

$$\zeta_{10\text{uniform}}(\xi, \Delta) = \frac{1}{2\Delta^{2/3}} G_{10}(Q_c(\xi)) \text{Ai}'\{\Delta^{2/3}\sigma(\xi)\}. \quad (4.10)$$

(This result can also be obtained by noting that (2.8) can be written in terms of the derivative of (2.7) with respect to  $\xi$ , for a suitable choice of  $\bar{\zeta}_E(\kappa)$ .)

The corresponding transitional approximation is

$$\zeta_{10\text{transitional}}(\xi, \Delta) = \frac{1}{2^{1/3}\Delta^{2/3}} \text{Im} \left( \frac{\bar{\zeta}_0(\kappa)}{\kappa} \right)_{\kappa=\sqrt{2(1-\xi)}} \text{Ai}'\{2^{1/3}\Delta^{2/3}(\xi - 1)\}. \quad (4.11)$$

### 4.3. Even initial velocity

A similar manipulation of (2.9), incorporating the fact that  $\bar{\zeta}_E(\kappa)$  vanishes quadratically at  $\kappa = 0$ , so that the integrand vanishes linearly at  $\kappa = 0$ , leads to

$$\zeta_{2\text{Euniform}}(\xi, \Delta) = -\text{Im} \frac{1}{2\pi} \int_0^\infty dQ Q G_{2E}(Q) \exp\{i\Delta(Q\sigma(\xi) + \frac{1}{3}Q^3)\}, \quad (4.12)$$

where

$$G_{2E}(Q) = \frac{d\kappa}{dQ} \frac{\bar{\zeta}_E(\kappa(Q))}{Q\sqrt{\kappa(Q)\tanh\kappa(Q)}}. \quad (4.13)$$

The function  $G_{2E}$  is finite over the whole integration range.

When  $Q$  is replaced by  $Q_c$ , the integral is again the derivative of the Airy function, giving the uniform approximation

$$\zeta_{2\text{Euniform}}(\xi, \Delta) = \frac{1}{2\Delta^{2/3}} G_{2E}(Q_c(\xi)) \text{Ai}'\{\Delta^{2/3}\sigma(\xi)\}. \quad (4.14)$$

This looks similar to the ‘elevation odd’ case (4.10), and indeed figures 1(b) and (c) look similar. But they are not the same, because of the  $1/\tanh$  factor in (4.13), and the resulting tsunami profiles are slightly different: in figure 1(b) the largest crest is the third, whereas in figure 1(c) it is the fourth.

The corresponding transitional approximation is

$$\zeta_{10\text{transitional}}(\xi, \Delta) = \frac{1}{2^{1/3}\Delta^{2/3}} \text{Im} \left( \frac{\bar{\zeta}_0(\kappa)}{\kappa} \right)_{\kappa=\sqrt{2(1-\xi)}} \text{Ai}'\{2^{1/3}\Delta^{2/3}(\xi - 1)\}. \quad (4.15)$$

#### 4.4. Odd initial velocity

This is very similar to the even initial elevation case, and the analysis of (2.10), similar to that in section 4.1, leads to

$$\zeta_{20\text{uniform}}(\xi, \Delta) = -\frac{1}{2}G_{20}(Q_c(\xi))\text{Ai}\{-\sigma(\xi)\}, \quad (4.16)$$

where

$$G_{20}(Q) = \frac{d\kappa}{dQ} \frac{\text{Im} \bar{\zeta}_0(\kappa(Q))}{\sqrt{\kappa(Q) \tanh \kappa(Q)}}. \quad (4.17)$$

This looks similar to the ‘elevation even’ case of section 4.1, explaining the similarity of figures 1(a) and (d).

Since both the numerator and denominator are proportional to  $Q$  as  $Q \rightarrow 0$ , the function  $G_{20}$  is finite at the origin.

Expansion about  $x = 1$  leads to the transitional approximation

$$\zeta_{20\text{transitional}}(\xi, \Delta) = -\frac{1}{(4\Delta)^{1/3}} \text{Im} \left( \frac{\bar{\zeta}_0(\sqrt{2(1-\xi)})}{\sqrt{2(1-\xi)}} \right) \text{Ai}\{2^{1/3} \Delta^{2/3}(\xi - 1)\}. \quad (4.18)$$

## 5. Uniform approximations for two-dimensional waves

### 5.1. Even initial elevation

So as not to be restricted to disturbances with circular symmetry, we start from the first of the equations (2.13), rather than (2.15). The first step in approximating this double integral is application of the method of stationary phase to the angular integral. The stationary-phase point is  $\phi_\kappa = \phi_\rho$ , selecting the plane wave travelling in the direction  $\mathbf{e}_\rho$  from the source to the point  $\rho$ . Thus

$$\zeta_{1\text{E}}(\rho, \Delta) \approx \frac{1}{\sqrt{8\pi^3 \rho \Delta}} \text{Re} \left[ \exp(-\frac{1}{4}i\pi) \int_0^\infty d\kappa \kappa^{1/2} \bar{\zeta}_\text{E}(\kappa \mathbf{e}_\rho) \exp\{i\Delta(\kappa\rho - \sqrt{\kappa \tanh \kappa})\} \right]. \quad (5.1)$$

Now we apply the map (3.2) (with  $\rho$  replacing  $\xi$ ) to get

$$\zeta_{1\text{E}}(\rho, \Delta) \approx \frac{1}{\sqrt{8\pi^3 \rho \Delta}} \text{Re} \left[ \exp(-\frac{1}{4}i\pi) \int_0^\infty dQ Q^{1/2} H_{1\text{E}}(Q) \exp\{i\Delta(Q\sigma(\rho) + \frac{1}{3}Q^3)\} \right], \quad (5.2)$$

where

$$H_{1\text{E}}(Q) = \frac{d\kappa}{dQ} \sqrt{\frac{\kappa}{Q}} \bar{\zeta}_\text{E}(\kappa(Q) \mathbf{e}_\rho). \quad (5.3)$$

As in the one-dimensional cases, the uniform approximation is obtained by replacing  $Q$  by  $Q_c(\rho)$  in the prefactor. But now the comparison integral is not simply an Airy function, because

of the factor  $Q^{1/2}$ ; instead, it is

$$I_1(X) = \frac{1}{(2\pi)^{3/2}} \operatorname{Re} \exp(-\frac{1}{4}i\pi) \int_0^\infty du u^{1/2} \exp\{i(\frac{1}{3}u^3 + Xu)\}. \quad (5.4)$$

However, this can be expressed in terms of Airy functions, as follows:

$$I_1(X) = -\frac{1}{\sqrt{2}} \operatorname{Ai}\left(\frac{X}{4^{1/3}}\right) \operatorname{Ai}'\left(\frac{X}{4^{1/3}}\right). \quad (5.5)$$

(To verify this result, simply replace each Airy function by its integral representation and then change variables in the resulting double integral—see also [13, 14]). In terms of  $I_1$ , the uniform approximation is

$$\zeta_{1\text{Uniform}}(\rho, \Delta) = \frac{1}{\Delta\sqrt{\rho}} H_{1\text{E}}(Q_c(\rho)) I_1(\Delta^{2/3}\sigma(\rho)). \quad (5.6)$$

The prefactor  $H_{1\text{E}}(Q_c)$  involves the derivative of the mapping at  $Q_c$ , which is given by (4.5) (with  $\rho$  replacing  $\xi$ ).

The transitional approximation, obtained from the uniform approximation by expansion for  $\rho \approx 1$ , is

$$\zeta_{1\text{Transitional}}(\rho, \Delta) = \frac{1}{\Delta} \sqrt{\frac{2}{\rho}} \bar{\zeta}_{\text{E}}(\mathbf{e}_\rho \boldsymbol{\kappa})_{\kappa=\sqrt{2(1-\rho)}} I_1\{(2\Delta^2)^{1/3}(\rho-1)\}. \quad (5.7)$$

As illustrated in figure 2(a), the uniform approximation reproduces the tsunami profile accurately over the whole range of significance. Further illustration of the accuracy is given in figure 5, which for  $h = 4$  km represents the propagation of an initial disturbance with a width of 2 km when the front has travelled 800 km. As figures 5(a)–(c) show, the uniform approximation cannot be distinguished from the exact profile over the entire range of significant elevation.

However, there are small deviations for small  $\rho$ , that is, near the source. These can be discerned in figure 2(a), and are clearly visible in the  $100 \times$  magnification in figure 5(d). The deviations consist of a small shift of the uniform approximation relative to the exact profile. This originates with a failure of the stationary-phase approximation for the angular integral, employed at the beginning of this section, to describe the small- $\kappa$  behaviour accurately. The true limiting small- $\rho$  behaviour for large  $\Delta$  is obtained from the small- $\kappa$  behaviour of the two-dimensional integral (2.13):

$$\begin{aligned} \zeta_{1\text{E}}(\rho, \Delta) &\xrightarrow{\rho \rightarrow 0} \frac{\bar{\zeta}_{\text{E}}(0)}{(2\pi)^2} \operatorname{Re} \int_0^{2\pi} d\phi_\kappa \int_0^\infty d\kappa \kappa \exp\{i\Delta\kappa(\rho\cos\phi_\kappa - 1)\} \\ &= -\frac{\bar{\zeta}_{\text{E}}(0)}{2\pi\Delta^2(1-\rho^2)^{3/2}}. \end{aligned} \quad (5.8)$$

As figure 5(d) illustrates, this fits the offset very accurately. Equation (5.8), for  $\rho \ll 1$ , can be combined with the uniform approximation (5.6) for larger  $\rho$ , so that the profile can be described over the whole range, but the improvement is in a region where the elevation is small for the large  $\Delta$  we are considering here and so is probably not worth incorporating.

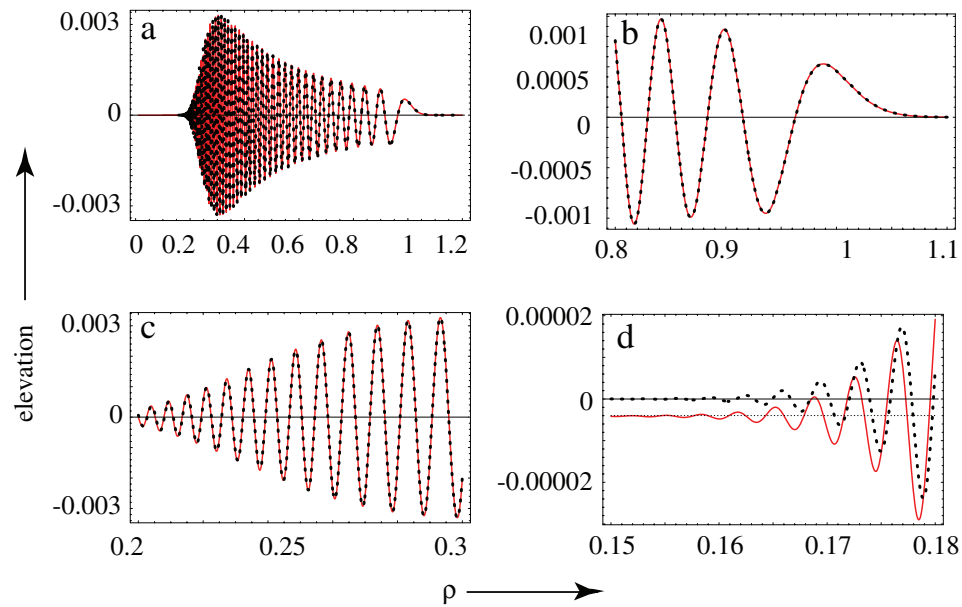


**Figure 5.** Two-dimensional tsunami profiles for  $\Delta = 200$  and  $w = 0.5$ , calculated for the Gaussian initial conditions (2.19), for even initial elevation. (a) Complete profile; (b) magnification of the front; (c) magnification of the tail; (d) magnification near the source. Full red curves, numerical computations of oscillatory integral (2.15) and dots, uniform asymptotic approximation (5.6), indistinguishable from the exact profiles except in (d) (note the factor of 100 vertical magnification as compared with (a)). The dotted line in (d) indicates the constant theoretical offset (5.8).

### 5.2. Odd initial elevation

From now on, the procedure will follow closely that of the previous section. Applying the method of stationary phase to the angular integral in the first of the equations (2.13) gives

$$\zeta_{10}(\rho, \Delta) \approx \frac{1}{\sqrt{8\pi^3 \rho \Delta}} \operatorname{Re} \left[ \exp(+\frac{1}{4}i\pi) \int_0^\infty d\kappa \kappa^{1/2} [\operatorname{Im} \bar{\zeta}_0(\kappa \mathbf{e}_\rho)] \exp\{i\Delta(\kappa\rho - \sqrt{\kappa \tanh \kappa})\} \right]. \quad (5.9)$$

Applying the map (3.2) gives

$$\zeta_{10}(\rho, \Delta) \approx \frac{1}{\sqrt{8\pi^3 \rho \Delta}} \operatorname{Re} \left[ \exp(+\frac{1}{4}i\pi) \int_0^\infty dQ Q^{3/2} H_{10}(Q) \exp\{i\Delta(Q\sigma(\rho) + \frac{1}{3}Q^3)\} \right], \quad (5.10)$$

where

$$H_{10}(Q) = \frac{d\kappa}{dQ} \sqrt{\frac{\kappa}{Q^3}} [\operatorname{Im} \bar{\zeta}_0(\kappa(Q) \mathbf{e}_\rho)]. \quad (5.11)$$

$H_{10}$  is finite at  $Q = 0$ , because  $\bar{\zeta}_0(\kappa)$  vanishes linearly as  $\kappa \rightarrow 0$ .

The comparison integral associated with (5.10) is the derivative of  $I_1(X)$  from the previous section, namely

$$I_2(X) = I_1'(X) = 2^{1/6} \left[ \frac{X}{4^{1/3}} \text{Ai} \left( \frac{X}{4^{1/3}} \right) \text{Ai}' \left( \frac{X}{4^{1/3}} \right) + \frac{1}{4} \text{Ai}^2 \left( \frac{X}{4^{1/3}} \right) \right], \quad (5.12)$$

and leads to the uniform approximation

$$\zeta_{1\text{Uniform}}(\rho, \Delta) = \frac{1}{\Delta^{4/3} \sqrt{\rho}} H_{10}(Q_c(\rho)) I_2(\Delta^{2/3} \sigma(\rho)). \quad (5.13)$$

The transitional approximation for this case is

$$\zeta_{1\text{Transitional}}(\rho, \Delta) = \frac{2^{5/6}}{\Delta^{4/3} \sqrt{\rho}} \left( \frac{\text{Im} \bar{\zeta}_0(\kappa \mathbf{e}_\rho)}{\kappa} \right)_{\kappa=\sqrt{2(1-\rho)}} I_2\{(2\Delta^2)^{1/3}(\rho-1)\}. \quad (5.14)$$

As illustrated in figure 2(b), the uniform approximation again reproduces the tsunami profile accurately over the whole range of significance. Again there are small deviations for small  $\rho$ , analogous to (5.8), and given for this case by

$$\zeta_{10}(\rho, \Delta) \xrightarrow{\rho \rightarrow 0} -\frac{3\rho}{2\pi\Delta^3(1-\rho^2)^{5/2}} (\text{Im} \bar{\zeta}_0(\kappa \mathbf{e}_\rho)/\kappa)_{\kappa=0}. \quad (5.15)$$

This could be combined with the uniform approximation (5.13), but again the advantage of this stratagem diminishes as  $\Delta$  increases.

### 5.3. Even initial velocity

Applying the method of stationary phase to the angular integral in the second of the equations (2.13) gives

$$\zeta_{2\text{E}}(\rho, \Delta) \approx \frac{1}{\sqrt{8\pi^3 \rho \Delta}} \text{Re} \left[ \exp(+\frac{1}{4}i\pi) \int_0^\infty \frac{d\kappa}{\sqrt{\tanh \kappa}} \bar{\zeta}_{\text{E}}(\kappa \mathbf{e}_\rho) \exp\{i\Delta(\kappa\rho - \sqrt{\kappa \tanh \kappa})\} \right]. \quad (5.16)$$

Applying the map (3.2) gives

$$\zeta_{2\text{E}}(\rho, \Delta) \approx \frac{1}{\sqrt{8\pi^3 \rho \Delta}} \text{Re} \left[ \exp(+\frac{1}{4}i\pi) \int_0^\infty dQ Q^{3/2} H_{2\text{E}}(Q) \exp\{i\Delta(Q\sigma(\rho) + \frac{1}{3}Q^3)\} \right], \quad (5.17)$$

where

$$H_{2\text{E}}(Q) = \frac{d\kappa}{dQ} \frac{1}{\sqrt{Q^3 \tanh \kappa}} \bar{\zeta}_{\text{E}}(\kappa(Q) \mathbf{e}_\rho). \quad (5.18)$$

$H_{2\text{E}}$  is finite at  $Q = 0$ , because  $\bar{\zeta}_{\text{E}}(\kappa)$  vanishes quadratically as  $\kappa \rightarrow 0$ .

The comparison integral associated with (5.17) is  $I_2(X)$  from the previous section (equation (5.12)), leading to the uniform approximation

$$\zeta_{2\text{Euniform}}(\rho, \Delta) = \frac{1}{\Delta^{4/3}\sqrt{\rho}} H_{2\text{E}}(Q_c(\rho)) I_2(\Delta^{2/3}\sigma(\rho)). \quad (5.19)$$

The transitional approximation for this case is

$$\zeta_{2\text{Etransitional}}(\rho, \Delta) = \frac{2^{5/6}}{\Delta^{4/3}\sqrt{\rho}} \left( \frac{\text{Im} \bar{\zeta}_{\text{E}}(\kappa \mathbf{e}_\rho)}{\kappa^2} \right)_{\kappa=\sqrt{2(1-\rho)}} I_2\{(2\Delta^2)^{1/3}(\rho-1)\}. \quad (5.20)$$

As illustrated in figure 2(c), the uniform approximation again reproduces the tsunami profile accurately over the whole range of significance. Again there are small deviations for small  $\rho$ , analogous to (5.8), and given for this case by

$$\zeta_{2\text{E}}(\rho, \Delta) \xrightarrow{\rho \rightarrow 0} -\frac{(2+\rho^2)}{2\pi\Delta^3(1-\rho^2)^{5/2}} \left( \frac{\bar{\zeta}_{\text{E}}(\kappa \mathbf{e}_\rho)}{\kappa^2} \right)_{\kappa=0}. \quad (5.21)$$

This could be combined with the uniform approximation (5.19), but the advantage of this stratagem diminishes as  $\Delta$  increases.

#### 5.4. Odd initial velocity

Applying the method of stationary phase to the angular integral in the second of the equations (2.13) gives

$$\zeta_{20}(\rho, \Delta) \approx -\frac{1}{\sqrt{8\pi^3\rho\Delta}} \text{Re} \left[ \exp(-\frac{1}{4}i\pi) \int_0^\infty \frac{d\kappa}{\sqrt{\tanh \kappa}} [\text{Im} \bar{\zeta}(\kappa \mathbf{e}_\rho)] \times \exp\{i\Delta(\kappa\rho - \sqrt{\kappa \tanh \kappa})\} \right]. \quad (5.22)$$

Applying the map (3.2) gives

$$\zeta_{20}(\rho, \Delta) \approx -\frac{1}{\sqrt{8\pi^3\rho\Delta}} \text{Re} \left[ \exp(-\frac{1}{4}i\pi) \int_0^\infty dQ Q^{1/2} H_{20}(Q) \exp\{i\Delta(Q\sigma(\rho) + \frac{1}{3}Q^3)\} \right], \quad (5.23)$$

where

$$H_{20}(Q) = \frac{d\kappa}{dQ} \sqrt{\frac{1}{Q \tanh \kappa}} [\text{Im} \bar{\zeta}_0(\kappa(Q) \mathbf{e}_\rho)]. \quad (5.24)$$

$H_{20}$  is finite at  $Q = 0$ , because  $\bar{\zeta}_0(\kappa)$  vanishes linearly as  $\kappa \rightarrow 0$ .

Now the comparison integral is  $I_1(X)$  from section 5.1 (equation (5.5)), leading to the uniform approximation

$$\zeta_{20\text{uniform}}(\rho, \Delta) = -\frac{1}{\Delta\sqrt{\rho}} H_{20}(Q_c(\rho)) I_1(\Delta^{2/3}\sigma(\rho)). \quad (5.25)$$

The transitional approximation for this case is

$$\zeta_{2\text{Otransitional}}(\boldsymbol{\rho}, \Delta) = -\frac{1}{\Delta} \sqrt{\frac{2}{\rho}} \left( \frac{\text{Im} \bar{\zeta}_0(\kappa)}{\kappa} \right)_{\kappa=\sqrt{2(1-\rho)}} I_1\{(2\Delta^2)^{1/3}(\rho-1)\}. \quad (5.26)$$

As illustrated in figure 2(d), the uniform approximation again reproduces the tsunami profile accurately over the whole range of significance. The deviation for small  $\rho$  behaviour (analogous to (5.13)) is

$$\zeta_{2\text{O}}(\boldsymbol{\rho}, \Delta) \xrightarrow{\rho \rightarrow 0} -\frac{(\text{Im} \bar{\zeta}_0(\kappa \mathbf{e}_\rho)/\kappa)_{\kappa=0} \rho}{2\pi \Delta^2 (1-\rho^2)^{3/2}}. \quad (5.27)$$

This could be combined with the uniform approximation (5.25), but again the advantage of this stratagem diminishes as  $\Delta$  increases.

## 6. Concluding remarks

The central results of this paper are the uniform asymptotic formulas (4.3), (4.10), (4.12) and (4.16) for the one-dimensional case, and (5.6), (5.13), (5.19) and (5.25) for the two-dimensional case. Numerical implementation is quick and very simple: it requires only the Airy function and its derivative, and the implicit function  $\kappa_c(\xi)$  defined by (3.1), which is common to all cases. The formulas were obtained in the asymptotic limit  $\Delta \gg 1$ , where  $\Delta$  is the distance of the front from the source, in units of the water depth  $h$ ; however they accurately reproduce the entire tsunami profile even when the front is quite close to the source.

Uniform asymptotics provide a quick and easy way to estimate the form of the travelling profile for a wide range of source conditions. However, application of the theory to the realistic modelling of tsunamis requires the relaxation of our assumption that the depth of the ocean is constant. Variations in the depth  $h(\mathbf{r})$  could be incorporated, assuming these are slow in comparison with the wavelengths in the tsunami profile, and will give rise to two effects.

The first is associated with depth variations along the direction of propagation (i.e. along the ‘water ray’—see [15]). Their main effect is to replace the arguments in the comparison functions ( $\text{Ai}$  and  $\text{Ai}'$ ) by the  $2/3$  power of the phase (Hamilton’s principal function) accumulated along the ray. This phase is

$$\gamma(\mathbf{r}, t) = \int_{\mathbf{r}_0}^{\mathbf{r}} (\mathbf{dr}' \cdot \mathbf{k}(\mathbf{r}', t)) - \omega(\mathbf{k}(\mathbf{r}, t), \mathbf{r}, t) t, \quad (6.1)$$

where  $\omega$  and  $\mathbf{k}$  are the frequency and wavevector of waves reaching  $\mathbf{r}$  at time  $t$ , determined by Hamilton’s equations with the dispersion relation (1.1) as Hamiltonian (there is no time integration in the second term because  $\omega$  is conserved during propagation).

The second effect is associated with depth variations transverse to the direction of propagation. Their main effect is to bend the tsunami rays. The curvature  $C$  associated with wavenumber  $k$  is most easily calculated from Hamilton’s equations, leading to

$$C(\mathbf{r}, k) = -\frac{\mathbf{n}(\mathbf{r}) \cdot \nabla_t \log h(\mathbf{r})}{\left(1 + \frac{\sinh[2kh(\mathbf{r})]}{2kh(\mathbf{r})}\right)}, \quad (6.2)$$

